

Luminescence and EPR studies of ultraviolet light emitting $\text{La}_2\text{Zr}_2\text{O}_7:\text{Gd}^{3+}$ phosphor powder

Vijay Singh¹ · G. Sivaramaiah² · J. L. Rao³ · R. Senthil Kumaran⁴ · Pramod K. Singh⁵ · Tae-Su Kim¹ · Lark Kyo Kim⁶

Received: 23 January 2015 / Accepted: 4 April 2015 / Published online: 12 April 2015
© Springer Science+Business Media New York 2015

Abstract The Gd^{3+} doped $\text{La}_2\text{Zr}_2\text{O}_7$ phosphor has been prepared by solution combustion method and characterized using powder X-ray diffraction, scanning electron microscopy, electron paramagnetic resonance (EPR) and photoluminescence spectroscopy. The EPR spectrum of Gd^{3+} doped $\text{La}_2\text{Zr}_2\text{O}_7$ exhibits resonance signals having effective g values at $g \approx 1.84, 1.93, 2.0, 3.00, 3.85$ and 6.12 . Upon UV light excitation (274 nm), the phosphor exhibits a strong and sharp UV emission at 312.5 nm, which is ascribed to ${}^6\text{P}_{7/2} \rightarrow {}^8\text{S}_{7/2}$ transition of Gd^{3+} ions. EPR and optical investigations of the sample confirm the presence of Gd^{3+} in the $\text{La}_2\text{Zr}_2\text{O}_7$ matrix.

1 Introduction

Recently, various pyrochlores of the basic formula $\text{A}_2\text{B}_2\text{O}_7$ (A = rare earth and B = Zr, Hf, Ti, or Sn) have been extensively investigated for their magnetic, optical and

electronic properties [1–4]. Pyrochlore type of rare-earth zirconium oxides ($\text{A}_2\text{Zr}_2\text{O}_7$, A = rare earth) are of considerable interest in recent years [5–7]. There is a considerable interest in $\text{A}_2\text{Zr}_2\text{O}_7$ because of possible applications as host materials for fluorescence centres, oxidation catalysts and high-temperature heating elements [5–10]. These rare-earth zirconium oxides have complex chemistry, low sintering, low thermal conductivity, high melting point, excellent stability and ability to accommodate defects. Several interesting pyrochlores, such as $\text{Gd}_2\text{Zr}_2\text{O}_7$, $\text{Sm}_2\text{Zr}_2\text{O}_7$, $\text{Nd}_2\text{Zr}_2\text{O}_7$ and $\text{La}_2\text{Zr}_2\text{O}_7$ were investigated [11–14]. It is found that, $\text{La}_2\text{Zr}_2\text{O}_7$ has excellent thermal stability, high phase stability, low thermal conductivity, low sintering rate, and become a very promising candidate for new potential applications [15, 16]. The pyrochlore of interest in the present study is lanthanum zirconium oxide ($\text{La}_2\text{Zr}_2\text{O}_7$). $\text{La}_2\text{Zr}_2\text{O}_7$ has a cubic pyrochlore structure. The crystal structure consists of the corner-shared ZrO_6 octahedra and La^{3+} ions fill the holes. There are vacancies randomly distributed at La^{3+} , Zr^{4+} and O^{2-} sites, which do not affect phase stability. Both La^{3+} and Zr^{4+} sites can be substituted by a lot of other elements with similar ionic radii. The luminescent properties of the trivalent rare-earth doped $\text{La}_2\text{Zr}_2\text{O}_7$ have been reported elsewhere [17–20].

Gadolinium is an important rare earth ion, which has been used as activator in various luminescent materials [21–23]. Besides of this Gd^{3+} doped phosphors can be effectively excited by X-ray and it is possible to observe the emission from higher levels like ${}^6\text{I}$ and ${}^6\text{G}$. Usually, Gd^{3+} emission in the phosphor shows sharp lines mainly at around 313 nm. Light in the wavelength range 280–315 nm is generally referred to as ultraviolet-B (UVB) radiation [24]. UVB is used in many applications such as photocopying and phototherapy [25]. During phototherapy investigations, it was noticed that UV in the narrow region

✉ Vijay Singh
vijayjiin2006@yahoo.com

¹ Department of Chemical Engineering, Konkuk University, Seoul 143-701, Republic of Korea

² Department of Physics, Government College for Men (Autonomous), Kadapa 516004, India

³ Department of Physics, Sri Venkateswara University, Tirupati 517502, India

⁴ Department of Biological Engineering, Konkuk University, Seoul 143-701, Republic of Korea

⁵ Materials Research Laboratory, School of Basic Sciences and Research, Sharda University, Greater Noida 201310, India

⁶ School of Electrical and Electronic Engineering, Shandong University of Technology, 12 Zhangzhou Road, Zibo 255091, Shandong, China

(300–320 nm) showed remarkable therapeutic effects [26]. UV emission in a narrow band centred at around 311 nm is thus required. The Gd doped phosphor materials are ideal for UVB emissions. It has been reported that UV therapy is useful for treating more than 40 types of skin diseases [27] and disorders. Therefore, there is indeed the need of UV emitting phosphor materials for phototherapy lamps.

The authors have selected Gd^{3+} as dopant since it is a stable ion in rare-earth ions as the hyperfine splitting is smaller. The orbital angular momentum is zero and it has exceptional special qualities among the rare-earth ions. Electron paramagnetic resonance (EPR) spectroscopy is one of the important spectroscopic methods that can be used for structural determination of transition metal and rare-earth ions in materials such as glasses and phosphors. The information obtained from this method is precise, accurate and perfect than the optical methods. It is used for predicting the oxidation states, nature of bonding, site symmetry between the dopant and the host lattice [28–30]. Therefore, luminescence studies must be combined with EPR for the full identification of the exact nature of dopant inside the host materials.

In the past several years, significant efforts have been devoted by several research groups towards the synthesis and characterization of impurity doped $La_2Zr_2O_7$ material [17–20, 31–33]. Nair et al. [34] studied preparation and characterization of lanthanum zirconate. Alaparthy et al. [35] studied europium doped lanthanum zirconate nanoparticles with high concentration quenching. They prepared these nanoparticles by a kinetically modified molten salt synthetic process. In the present work, we have succeeded in preparing Gd^{3+} doped $La_2Zr_2O_7$ by combustion process. To the best of our knowledge, no reports are present for Gd^{3+} ions doped in $La_2Zr_2O_7$ phosphor using the present experimental methods. The XRD was performed for knowing the structure of the phosphor. The EPR was conducted at room temperature and 123 K for knowing the structural environment between the dopant and the phosphor lattice. From EPR studies, the zero-field splitting parameter was determined. The photoluminescence studies were performed at room temperature for knowing the excited state properties of Gd^{3+} ions in this phosphor.

2 Materials preparation and analysis

We prepared sample of Gd doped $La_2Zr_2O_7$ phosphor utilizing the combustion process. The process involves the exothermic reaction of an oxidizer (metal nitrate) and an organic fuel [urea (NH_2CONH_2)]. The energy released due to the exothermic reaction between the metal nitrates and fuel can rapidly heat the system to high temperatures without an external heat source. The precursors used were

3.2403 g of $La(NO_3)_3 \cdot 6H_2O$, 2.00 g of $ZrO(NO_3)_2 \cdot 2H_2O$, 0.0844 g of $Gd(NO_3)_3 \cdot 6H_2O$ and 2.7776 g of NH_2CONH_2 . The high-purity metal nitrates and urea were dissolved in deionized water in a Pyrex dish of approximately 200 ml capacity according to the chemical formula $La_2Zr_2O_7 \cdot Gd_{(0.05)}$. The solution was allowed to react at 353 K for 30 min to obtain a homogenous solution. Then the solution was introduced into a muffle furnace preheated to 823 K. The water quickly evaporated and the mixture formed a foam, within which a vigorous reaction between the nitrates and urea soon initiated and ended. The entire combustion process was completed in about 3–5 min. The glass beaker was taken out from the furnace and the fluffy masses were crushed into a fine powder. The powder was transferred into 50 ml alumina crucibles to be heat-treated to 1273 K for 4 h. The resulting powder was then further used for characterization.

Powder XRD pattern was recorded in the 2θ range from 5° to 80° on a Philips X'Pert X-ray diffractometer with graphite monochromatized CuK_α radiation and nickel filter at a scanning step of 0.03° . Powder morphology was studied using Scanning Electron Microscopy (Hitachi S-3200N, Japan). The EPR spectra of the sample were recorded on a JEOL FE1X ESR Spectrometer, operating at the X-band frequencies, with a field modulation of 100 kHz. Emission and excitation spectra were recorded using a Fluorolog 3-22 Spectrofluorometer (Jobin Yvon) with a xenon lamp as an excitation source.

3 Results and discussion

3.1 XRD phase analysis

Figure 1 shows the XRD pattern of the $La_2Zr_2O_7:Gd^{3+}$ phosphor powder. The observed XRD pattern clearly indicates that the pure cubic crystal phase diffraction peaks of parent $La_2Zr_2O_7$ are matched well with the JCPDS data file (no. 73-0444). No other phase or unreacted starting material was observed. The diffraction pattern indicates that doping with gadolinium ions has a negligible effect on the diffraction pattern. As indicated by the XRD pattern that the crystallinity and cubic phase of $La_2Zr_2O_7$ could be obtained by the combustion synthesis.

3.2 Scanning electron microscopy studies

Low and high magnification scanning electron microscope (SEM) images of combustion synthesized $La_2Zr_2O_7:Gd^{3+}$ powders are shown in Fig. 2. Figure 2A displays the overall morphology of the samples, from which it can be clearly observed that the crystallites have no uniform size and shape. There is some portion with voids and pores

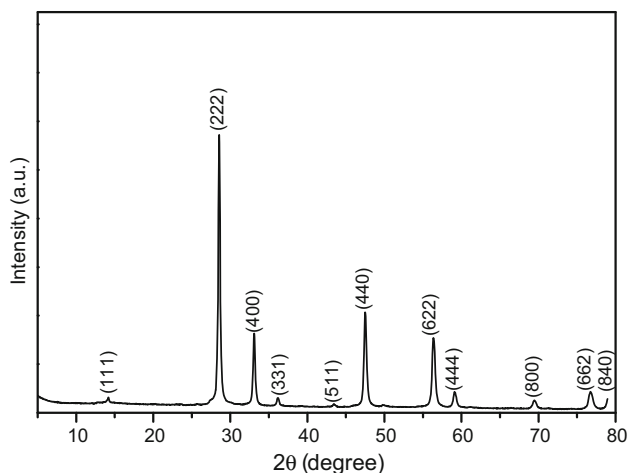


Fig. 1 Powder XRD pattern of $\text{La}_2\text{Zr}_2\text{O}_7:\text{Gd}^{3+}$ phosphor

while some do not. Due to the uncontrolled dynamics of the combustion reaction, these irregularities in sizes, shapes and porosity is occurred. Porosity could be expected in combustion derived product because of evolution of large amounts of gas during reaction. This porosity can be seen in Fig. 2B [magnified view of Fig. 2A (zone a)]. Interestingly, small particles near the pores can be seen in Fig. 2D [magnified view of Fig. 2B (zone b)]. Figure 2C is a magnified view of Fig. 2A (zone a') and Fig. 2E is a magnified view of Fig. 2C (zone c). The surface of the faceted plates is not smooth, and is actually composed of numerous nanoparticles, which can be vividly demonstrated by the enlarged SEM image shown in Fig. 2E.

3.3 Electron paramagnetic resonance studies

It is to be noted that EPR is an amenable and extensive technique to study transition metal ions and rare-earth ions in glasses, crystals, phosphors and minerals [36, 37]. This method is used for studying the bonding, and interactions with the lattice environments. Also, EPR is a non-destructive and non-invasive technique. The ground state properties of paramagnetic ions can be predicted using this vital method.

The electronic configuration of Gd^{3+} ion is $4f^7$ and its ground state is $^8S_{7/2}$. The characteristics of Gd^{3+} ions were different when compared with the other rare-earth ions because of zero angular momentum. The effective spin quantum number is $S = 7/2$ and also $I = 7/2$. Therefore eight hyperfine lines can be expected in EPR signals. The eightfold degenerate energy level of Gd^{3+} when placed in this phosphor is split into four Krammers' doublets. The EPR spectrum consists of four signals from one of the seven fine structure results from both interdoubtlet and intradoubtlet transitions. In the present case, the signals were

raised from one hyperfine line. The signals were not observed from the remaining seven hyperfine lines. The obtained spectrum is the most frequent signature of S state rare-earth ion in a low symmetry site. It is well established in many studies that the spectral characteristics strongly depend on the relative magnitude of Zeeman microwave frequency and the ligand field strength. When the microwave frequency is smaller when compared with the ligand field strength, the signals of Gd^{3+} are observed in the range $g > 2.0$. When the microwave frequency is of the same order as that of the ligand field strength, zero-field resonance is seen. If the microwave frequency is larger than the ligand field strength, the signals will be observed near $g \approx 2.0$. The spin–lattice relaxation time is longer and therefore the EPR signals can be observed even at room temperature. Spin–spin interaction between the nearest Gd ions leads to number of signals in the spectrum. The interaction with next nearest neighbours can lead to broadening of the signals. The EPR spectra of rare-earth ions in disordered materials are highly anisotropic and sensitive to variations in ligand field from site to site. It is known that the Gd^{3+} ion prefers to be 6 or 8 coordinated and can be more readily accommodated in a vitreous phase than in a crystalline state of higher symmetry.

Figure 3 shows EPR spectra observed at room temperature and 123 K. The spectra exhibited the signals with the effective g values at $g \approx 1.84, 1.93, 2.0, 3.0, 3.85$ and 6.12 . The g values are independent of temperature variation indicating that the structural environment between the Gd^{3+} ions and the phosphor lattice is invariant with the temperature variation. The signals at $g \approx 1.84, 1.93$ and 2.0 were attributed to weak cubic symmetry field between Gd^{3+} ions and the phosphor lattice [38, 39]. The signal at $g \approx 3.00$ was attributed to intermediate cubic symmetry field between the Gd^{3+} ions and the phosphor lattice [38, 39]. The signal at $g \approx 3.85$ was due to vitreous structure and disordered polycrystalline nature of this phosphor [38]. The signal at $g \approx 6.12$ was attributed to strong cubic symmetry field between the Gd^{3+} ions and the phosphor lattice [38, 39].

Rada et al. [38] investigated EPR studies of borotellurite glass ceramics. They observed six resonance signals at $g \approx 2.0, 2.8, 3.3, 4.3, 4.8,$ and 6.0 . The signals at $g \approx 2.0, 2.8, 6.0$ were attributed to weak, intermediate and strong cubic symmetry field between the dopant and the glass ceramic lattice. The signals at $g \approx 3.3, 4.3$ were attributed to the vitreous structure and disordered polycrystalline nature. The asymmetric absorption line at $g \approx 4.8$ has been attributed to orthorhombic symmetry in strong crystal field sites with coordination number lower than six. Murali et al. [40] studied the EPR studies of Gd^{3+} ions in lithium tetraborotellurite and lithium lead tetraborotellurite glasses. Their spectra exhibited broad EPR signals at $g \approx 2.0, 2.8$

Fig. 2 SEM micrographs of $\text{La}_2\text{Zr}_2\text{O}_7:\text{Gd}^{3+}$ phosphor. A magnified portion of **A** [blue rectangular marked, portion (a)] is shown in **B**. A magnified portion of **A** [red rectangular marked, portion (a')] is shown in **C**. Similarly, a magnified portion of **B** [green rectangular marked, portion (b)] is shown in **D** and a magnified portion of **C** [yellow rectangular marked, portion (c)] is shown in **E** (Color figure online)

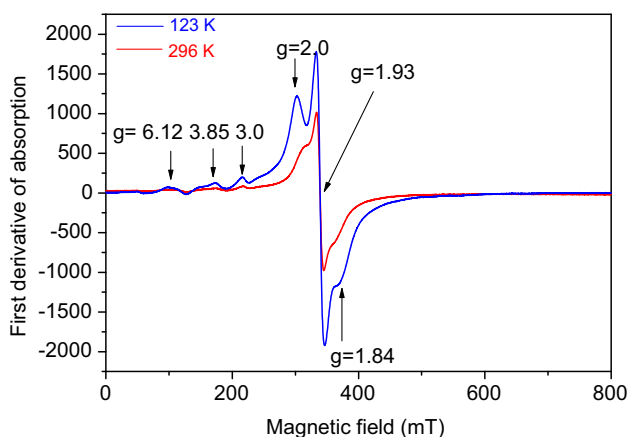
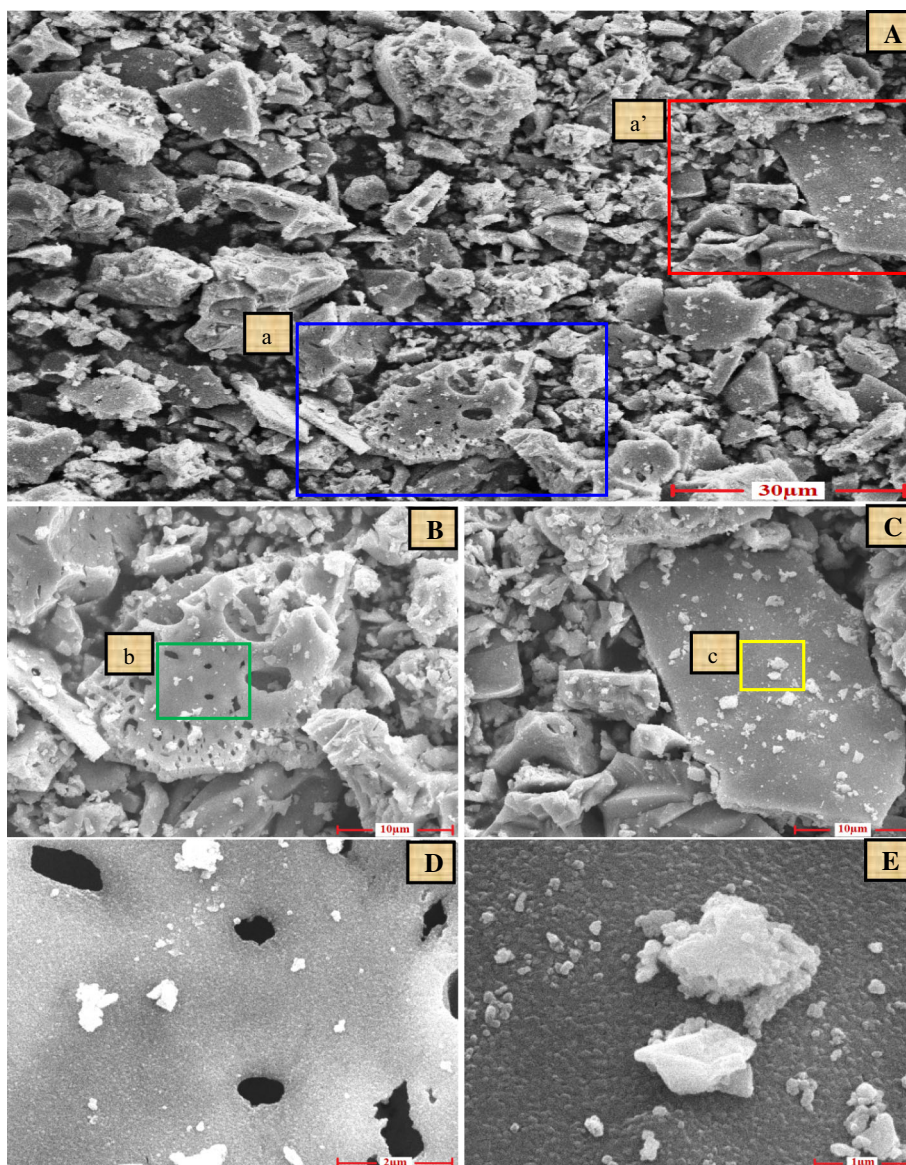


Fig. 3 EPR spectrum of $\text{La}_2\text{Zr}_2\text{O}_7:\text{Gd}^{3+}$ phosphor at 296 and 123 K

and 5.4. These signals were attributed to weak, intermediate and strong cubic symmetry fields between the dopant and the glass lattice. Vetter et al. [41] studied Gd^{3+} ions doped aluminium nitride using cathode luminescence and time resolved cathode luminescence. Thakare et al. [42] studied Gd^{3+} ions doped UV emitting phosphors. They studied photoluminescence properties of Gd^{3+} doped phosphors for narrow-range UVB lamps. Li et al. [43] studied luminescence and energy transfer properties of Gd^{3+} in $\text{LaAlGe}_2\text{O}_7$. Rao et al. [44] performed EPR study of Gd doped $\text{La}_2\text{Zr}_2\text{O}_7$ in bulk and nanosize at room temperature. The spectrum resembles with the typical U spectrum with the effective g values at $g \approx 5.6\text{--}6.0$, $2.8\text{--}2.9$ and $1.99\text{--}2.0$. They also observed the signals with the effective g values at $g \approx 4.0\text{--}4.2$, $2.2\text{--}2.3$. The U spectrum changes into single

peak with $g \approx 2.0$ as the particle size increases. In the investigation of U spectrum, the average over the distribution of crystal field parameters must be considered. The EPR absorption curve of the U spectrum has its' maximum near $g \approx 2.0$. On the other hand, there is wide range of crystal field strengths, where neither the Zeeman interaction nor the crystal field interaction may be treated by perturbation methods. The splittings arise from higher order perturbations involving spin–orbit coupling and spin–spin coupling. Kripal and Misra [45] studied EPR and optical investigations on Gd^{3+} ions in ammonium hydrogen malonate (AHM) single crystals. The EPR spectra recorded by them showed the presence of four magnetically inequivalent Gd^{3+} ions which belong to eight physically equivalent Gd^{3+} ions. Prokhorov et al. [46] studied the temperature and pressure dependences of EPR spectra of Gd^{3+} ion doped in the $EuAl_3(BO_3)_4$ monocrystal. They studied the ground state of Gd^{3+} ions substituting for Eu^{3+} in the $EuAl_3(BO_3)_4$ single crystal in the temperature range 300–4.2 K. The EPR spectra were analysed using the spin-Hamiltonian of an axial symmetry and observed the g value as 1.981. Recently, Gedam [47] studied optical study of Gd^{3+} ions in $KZnSO_4Cl:Ce^{3+}$ phosphor. Sivaramaiah et al. [48] studied ESR studies of Gd^{3+} ions in calcium tungsten, calcium tungsten copper phosphors. They observed the signals with the effective g values at $g \approx 13.76, 6.17, 3.68, 2.92, 2.78, 2.38, 2.12, 1.98, 1.70, 1.58, 1.46$ and 1.38 . These types of large number of g values are due to anisotropic nature of this phosphor.

The EPR spectrum is called U spectrum because of its omnipresence in vitreous materials as well as in disordered materials [49]. The explanation of U spectrum has been the subject of significant importance. Chepeleva and Lazukin [50] attributed the signal at $g \approx 6.0$ to a strong cubic crystal field which was also further explained by Nickin et al. [51]. Cugunov and Kliava [52] attributed the $g \approx 6.0$ peak to rhombic crystal field and broad signal with $g \approx 2.0$ to clusters of Gd^{3+} ions. Koopmans' et al. [53] decided that $g \approx 6.0$ signal is due to the Gd^{3+} sites of axial symmetry with intermediate crystal field strength [53]. The signal with $g \approx 2.0$ has been attributed to isolated rare earth ions [53]. A reasonable explanation for the analysis of "U spectrum" was given by Brodbeck and Iton [54]. According to them, the U spectrum will be observed when S-state rare earth ion has a large coordination number within the lattice. The signal at $g \approx 2.0$ is attributed to paramagnetic ions in sites characterized by relatively weak ligand fields, for which Zeeman term dominates. The signals with $g > 2$ are attributed to paramagnetic ions in sites of relatively strong ligand field, where the ligand field terms are comparable or larger than the Zeeman term [54].

The zero-field splitting parameter (D) can be calculated using the expression $D \approx \Delta B/6$ [55]. ΔB is the line width

between the central line and the edge line of the lower magnetic field in the EPR spectrum. The calculated D value is found to be 38.5 and 40.2 mT at 296 and 123 K respectively. The zero-field splitting (zfs) arises due to the spin–orbit and electronic spin–spin couplings [56]. The zfs is the removal of spin state degeneracy with $S > 1/2$ in the absence of an applied magnetic field. The zfs is represented by the letter D and is in axial form. Singh et al. [57] calculated the zfs parameter as 36.2 and 37 mT at 296 and 110 K respectively. Thus the determined value is consistent with the value reported in literature. The zfs is slightly increased with the decrease of temperature from 296 to 110 K.

3.4 Photoluminescence studies

Rare-earth ions doped materials such as phosphors have attracted much attention due to their excellent luminescence properties. The emission transitions give sharp lines with efficiency in the UV and visible region. UV-emitting phosphors find uses in various applications, such as photocopying, phototherapy, sun tanning, photocopying lamps, photoluminescent liquid crystal displays and radio photoluminescence. Kripal and Misra [45] studied the optical spectra of AHM single crystal. They observed five bands at 32,786, 36,067, 38,408, 43,992 and 48,540 cm^{-1} , respectively. The first three bands were attributed to ${}^6P_{5/2}$, ${}^6I_{11/2}$, and ${}^6D_{9/2}$. The fourth and fifth bands were attributed to ${}^6D_{5/2}$ and 6G levels respectively. Paksis et al. [58] investigated the energy levels and crystal field of $LaCl_3:Gd$. They observed the optical absorption bands in the region 32,100–40,580 cm^{-1} .

Figure 4A shows the excitation spectrum of $La_2Zr_2O_7:Gd^{3+}$ phosphor observed at 296 K when the emission wavelength is fixed at 312.5 nm. This spectrum exhibits a broad band around 242 nm, two intense bands centered at 274 and 276.5 nm (36,496, 36,166 cm^{-1}) and two weak bands centered at 253.8 and 279.8 nm (39,401, 35,778 cm^{-1}) in the UV region. The wide and broad band around 242 nm is most likely due to combination of the host lattice excitation and weak Gd^{3+} band. Previous investigation [43] on ultraviolet-emitting Gd doped phosphors show weak band around 242 nm. The observed excitation band positions and their assignments are shown in Table 1. Also, obtained results are in good agreement with the optical absorption band positions reported for Gd^{3+} ions in the literature [59, 60]. All transitions start from the ground state ${}^8S_{7/2}$ of the $4f^7$ configuration of Gd^{3+} ions. The excited states observed are 6I and 6D . The absorption bands for Gd^{3+} ions are very sharp and the strongest transitions are those to the 6I levels. Figure 4B shows the emission spectrum observed in the UV region when the excitation wavelength is fixed at 274 nm. The

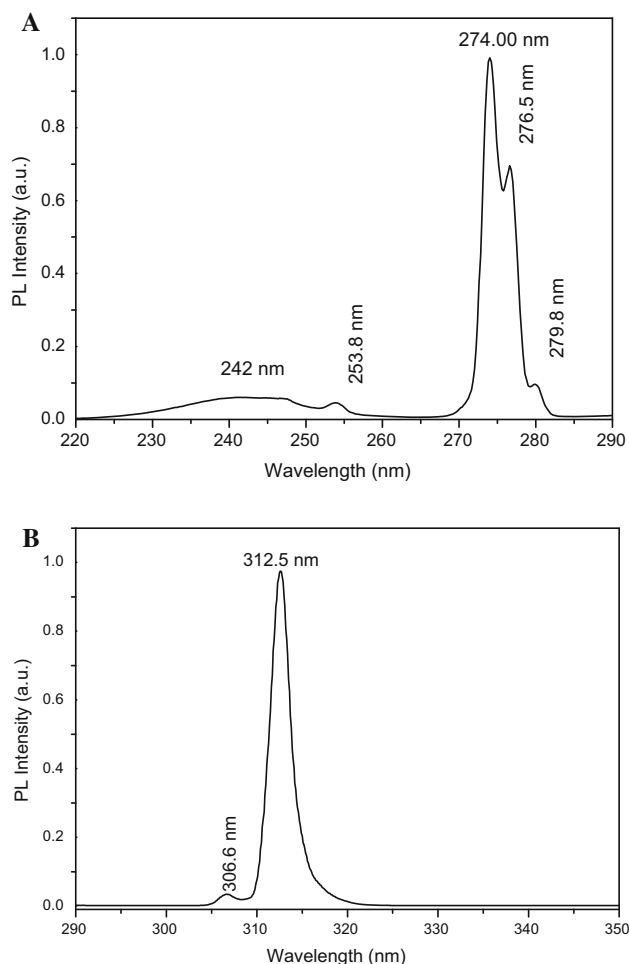


Fig. 4 Photoluminescence spectra of $\text{La}_2\text{Zr}_2\text{O}_7$ phosphor. **A** Excitation spectrum of $\text{La}_2\text{Zr}_2\text{O}_7:\text{Gd}^{3+}$ ($\lambda_{\text{em}} = 312.5$ nm) and **B** emission spectrum of $\text{La}_2\text{Zr}_2\text{O}_7:\text{Gd}^{3+}$ ($\lambda_{\text{ex}} = 274$ nm)

Table 1 The observed band positions along with their assignments for $\text{La}_2\text{Zr}_2\text{O}_7:\text{Gd}^{3+}$ [59, 60]

Transition from $^8\text{S}_{7/2}$ to	Observed band positions	
	Wavelength (nm)	Wavenumber (cm^{-1})
$^6\text{I}_{7/2}$	279.8	35,778
$^6\text{I}_{9/2}$	276.5	36,166
$^6\text{I}_{11/2}$	274	36,496
$^6\text{D}_{9/2}$	253.8	39,401

emission spectrum exhibits an intense narrow band centered at 312.5 nm ($32,000 \text{ cm}^{-1}$) and a weak band at 306.6 nm ($32,616 \text{ cm}^{-1}$). The intense peak observed at 312.5 nm ($32,000 \text{ cm}^{-1}$) in emission spectrum has been attributed to $^8\text{P}_{7/2} \rightarrow ^8\text{S}_{7/2}$ transition of Gd^{3+} ions [60]. It has long been known that the narrow UVB emitting phosphors are important for production of phototherapy lamps. The weak band observed at 306.6 nm

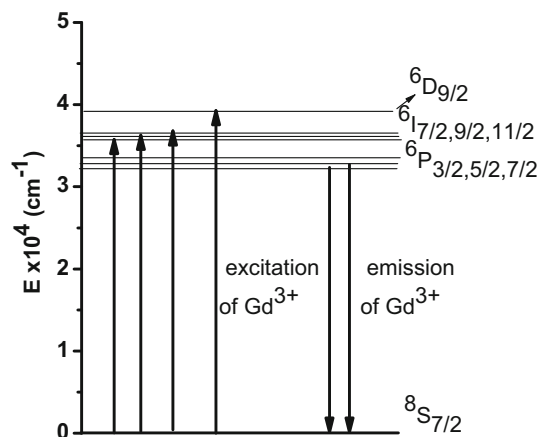


Fig. 5 Energy level diagram of Gd^{3+} ions in $\text{La}_2\text{Zr}_2\text{O}_7$ phosphor

($32,616 \text{ cm}^{-1}$) in emission spectrum has been attributed to $^8\text{P}_{5/2} \rightarrow ^8\text{S}_{5/2}$ transition of Gd^{3+} ions [60]. The energy level diagram of $\text{La}_2\text{Zr}_2\text{O}_7:\text{Gd}^{3+}$ ions are shown in Fig. 5. From this figure, it is observed that the $^6\text{P}_j$ and $^6\text{I}_j$ levels are closely spaced and $^6\text{D}_{9/2}$ is a little bit widely spaced from $^6\text{P}_j$ and $^6\text{I}_j$ energy levels. The effective ionic radii of Gd^{3+} and La^{3+} ions are 0.94 Å and 1.06 Å respectively. Therefore it may be reasonable to assume that Gd^{3+} ions incorporated at La^{3+} sites in this phosphor. In the Eu^{3+} -doped $\text{La}_2\text{Zr}_2\text{O}_7$, Eu^{3+} is assumed to replace the site of La^{3+} in the D_{3d} crystalline field, because of the same valence and similar ion radius [19].

4 Conclusions

To conclude, $\text{La}_2\text{Zr}_2\text{O}_7:\text{Gd}^{3+}$ powder phosphor was prepared using solution method. This method is able to produce single phase of $\text{La}_2\text{Zr}_2\text{O}_7$ phosphor. X-ray diffraction pattern reveals the formation of cubic crystal structure of $\text{La}_2\text{Zr}_2\text{O}_7:\text{Gd}^{3+}$ phosphor. Scanning electron microscopic reveals plates are not smooth, and is actually composed of numerous nanoparticles. EPR spectrum exhibits several resonance signals characteristic of Gd^{3+} ions. The signals with the effective g values at $g = 1.84, 1.93, 2.00$ were attributed to Gd^{3+} ions in weak cubic symmetry field. The signals with the effective g values at $g = 3.0, 3.85$ and 6.12 were attributed to Gd^{3+} ions in intermediate, vitreous structure and strong cubic symmetry field. The excitation spectrum exhibits bands characteristic of Gd^{3+} ions. The emission spectrum exhibits sharp band in the UV region centered at 312.5 nm and is ascribed to $^6\text{P}_{7/2} \rightarrow ^8\text{S}_{7/2}$ transition of Gd^{3+} ions.

Acknowledgments This paper was supported by the KU Research Professor Program of Konkuk University, Seoul (South Korea).

References

1. Y.H. Li, J. Wen, Y.Q. Wang, Z.G. Wang, M. Tang, J.A. Valdez, K.E. Sickafus, Nucl. Instrum. Methods B **287**, 130 (2012)
2. Y.H. Lee, H.S. Sheu, H.-C.I. Kao, Mater. Chem. Phys. **124**, 145 (2010)
3. B.P. Mandal, A. Banerji, V. Sathe, S.K. Deb, A.K. Tyagi, J. Solid State Chem. **180**, 2643 (2007)
4. J. Lian, L.M. Wang, R.G. Haire, K.B. Helean, R.C. Ewing, Nucl. Instrum. Methods B **218**, 236 (2004)
5. K.-J. Hu, Z.-G. Liu, J.-Y. Wang, C. Zhu, J.-H. Ouyang, J. Alloy. Compd. **576**, 177 (2013)
6. L. Liu, Z. Ma, F.-C. Wang, S.-Z. Zhu, Q. Xu, Rare Metal. Mater. Eng. **41**, 483 (2012)
7. S. Li, Z.-G. Liu, J.-H. Ouyang, Int. J. Appl. Ceram. Technol. **9**, 149 (2012)
8. Masayoshi. Uno, Atsuko. Kosuga, Mihoko. Okui, Kentarou. Horisaka, Hiroaki. Muta, Ken. Kurosaki, Shinsuke. Yamanaka, J. Alloy. Compd. **420**, 291 (2006)
9. K.E. Sickafus, L. Minervini, R.W. Grimes, J.A. Valdez, M. Ishimaru, F. Li, K.J. McClellan, T. Hartmann, Science **289**, 748 (2000)
10. A. Chaudhry, A. Canning, R. Boutchko, M.J. Weber, N. Grnbech-Jensen, S.E. Derenzo, J. Appl. Phys. **109**, 083708 (2011)
11. Z.-G. Liu, J.-H. Ouyang, Y. Zhou, X.L. Xia, Mater. Des. **30**, 3784 (2009)
12. O. Fabricnaya, M.J. Kriegel, J. Seidel, G. Savinykh, L.P. Ogorodova, I.A. Kiseleva, H.J. Seifert, Thermochim. Acta **526**, 50 (2011)
13. A.T. Nelson, M.M. Giachino, J.C. Nino, K.J. McClellan, J. Nucl. Mater. **444**, 385 (2014)
14. S. Yugeswaran, A. Kobayashi, B. Selvan, P.V. Ananthapadmanabhan, Vacuum **88**, 139 (2013)
15. X.Q. Cao, R. Vassen, W. Jungen, S. Schwartz, F. Tietz, D. Stöver, J. Am. Ceram. Soc. **84**, 2086 (2001)
16. K. Bobzin, E. Lugscheider, N. Bagecivan, High Temp. Mater. Process. **10**, 45 (2006)
17. Beichen. Duan, Jiachi. Zhang, Xue. Liu, Qi. Yuan, Yuhua. Wang, J. Alloy. Compd. **587**, 318 (2014)
18. K. Holliday, S. Finkeldei, S. Neumeier, C. Walther, D. Bosbach, T. Stumpf, J. Nucl. Mater. **433**, 479 (2013)
19. A. Zhang, M. Lü, G. Zhou, S. Wang, Y. Zhou, J. Phys. Chem. Solids **67**, 2430 (2006)
20. Y. Tong, S. Zhao, W. Feng, L. Ma, J. Alloy. Compd. **550**, 268 (2013)
21. S. Hachani, B. Moine, A. El-akrmi, M. Férid, Opt. Mater. **31**, 678 (2009)
22. H. Kondo, T. Hirai, S. Hashimoto, J. Lumin. **94–95**, 311 (2001)
23. I. Kudryavtseva, P. Liblik, A. Lushchik, A. Maaros, E. Vasil'chenko, Z. Azmaganbetova, T. Nurakhmetov, B. Toxanbayev, J. Lumin. **129**, 1890 (2009)
24. R.M. MacKie, Radiat. Prot. Dosim. **91**, 15 (2000)
25. R.C. Ropp, *Luminescence and the Solid State* (Elsevier, Amsterdam, 1991)
26. J.A. Parrish, K.F. Jaenicke, J. Invest. Dermatol. **76**, 359 (1981)
27. W.L. Morison, Semin. Cutan. Med. Surg. **18**, 297 (1999)
28. V. Singh, R.P.S. Chakradhar, J.L. Rao, D.-K. Kim, J. Lumin. **129**, 755 (2009)
29. V. Singh, V. Natarajan, J.-J. Zhu, Opt. Mater. **29**, 1447 (2007)
30. T.K. Gundu Rao, S.V. Moharil, Radiat. Meas. **42**, 35 (2007)
31. Chunjie. Wang, Yue. Wang, Xizhi. Fan, Wenzhi. Huang, Binglin. Zou, Xueqiang. Cao, Surf. Coat. Technol. **212**, 88 (2012)
32. Q. Du, G. Zhou, H. Zhou, Z. Yang, Opt. Mater. **35**, 257 (2012)
33. J. Zhang, Y. Jishun, X. Cheng, S. Hou, J. Alloy. Compd. **525**, 78 (2012)
34. J. Nair, P. Nair, E.B.M. Doesburg, J.G. Vanommen, J.R.H. Ross, A.J. Burggraaf, F. Mizukami, J. Mater. Sci. **33**, 4517 (1998)
35. S.B. Alaparathi, L. Lu, Y. Tian, Y. Mao, Mater. Res. Bull. **49**, 114 (2014)
36. A. Abragam, B. Bleaney, *Electron Paramagnetic Resonance of Transition Ions* (Clarendon Press, Oxford, 1970)
37. S.A. Al'tshuler, B.M. Kozyrev, *Electron Paramagnetic Resonance in Compounds of Transition Elements* (Wiley, New York, 1974)
38. S. Rada, V. Dan, M. Rada, E. Culea, J. Non-Cryst. Solids **356**, 474 (2010)
39. D.L. Griscom, J. Non-Cryst. Solids **40**, 211 (1980)
40. A. Murali, R.P.S. Chakradhar, J.L. Rao, Phys. B **364**, 142 (2005)
41. Ulrich. Vetter, Jan. Zenneck, Hans. Hofsäss, Appl. Phys. Lett. **83**, 2145 (2003)
42. D.S. Thakare, S.K. Omanwar, P.L. Muthal, S.M. Dhopte, V.K. Kondawar, S.V. Moharil, Phys. Status Solidi (a) **201**, 574 (2004)
43. Y.-C. Li, Y.-H. Chang, Y.-S. Chang, Y.-J. Lin, C.-H. Laing, J. Phys. Chem. C **111**, 10682 (2007)
44. K.K. Rao, N. Anantharamulu, M. Salagram, M. Vithal, Spectrochem. Acta Part A **66**, 646 (2007)
45. R. Kripal, I. Mishra, Phys. B **405**, 425 (2010)
46. A.D. Prokhorov, A.A. Prokhorov, L.F. Chernysh, V.P. Dyakonov, H. Szymczak, J. Magn. Magn. Mater. **323**, 1546 (2011)
47. S.C. Gedam, Res. J. Eng. Sci. **1**, 6 (2013)
48. G. Sivaramaiah, S. Sailaja, J.L. Rao, B. Sudhakar Reddy, Proc. Insa. **79**, 153 (2013)
49. L.E. Iton, C.M. Brodbeck, S.L. Suib, G.D. Stucky, J. Chem. Phys. **79**, 1185 (1983)
50. I.V. Chepeleva, V.N. Lazukin, Dokl. Akad. Nauk SSSR **226**, 311 (1976)
51. R.C. Nicklin, J.K. Johnstone, R.G. Barnes, D.R. Wilder, J. Chem. Phys. **59**, 1652 (1973)
52. L. Cugunov, J. Kliava, J. Phys. C **15**, L933 (1982)
53. H.J.A. Koopmans, M.M. Eprk, B. Nieuwenhuijse, P.J. Gellings, Phys. Status Solidi (b) **120**, 745 (1983)
54. C.M. Brodbeck, L.E. Iton, J. Chem. Phys. **83**, 4284 (1985)
55. C. Rudowicz, Magn. Res. Rev. **13**, 1 (1987)
56. C. Rudowicz, S.K. Misra, Appl. Spectrosc. Rev. **36**, 11 (2001)
57. V. Singh, G. Sivaramaiah, J.L. Rao, S.J. Dhoble, S.H. Kim, J. Electron. Mater. **44**, 121 (2015)
58. A.H. Piksis, G.H. Dieke, H.M. Crosswhite, J. Chem. Phys. **47**, 5083 (1967)
59. K. Binnemans, C. Görrler-Walrand, J.L. Adam, Chem. Phys. Lett. **280**, 333 (1997)
60. V. Singh, G. Sivaramaiah, J.L. Rao, S.H. Kim, Phys. B **416**, 101 (2013)